
Article:
Salmon Guzman, F., Jackson, M., Jones, S. et al. (1 more author) (2018) Use of digital image correlation to measure strain recovery in particle toughened thermoset resins. Strain, 54 (2). e12261. ISSN 0039-2103

https://doi.org/10.1111/str.12261

Use of digital image correlation to measure strain recovery in particle toughened thermoset resins

F. Salmon-Guzman[1], M. Jackson[2], S. Jones[2] and R. A. Tomlinson[1]*
[1]*Department of Mechanical Engineering, The University of Sheffield, UK*
[2]*Cytec Solvay Group, UK*

Abstract

A methodology for finding the yield point of epoxy resins, both neat and particulate toughened, is described. Trends of the effect that particulate filling has on the time dependent response of these materials were constructed from observations made with stereo-based digital image correlation (3D-DIC), namely, creep and stress relaxation at constant load. The use of 3D-DIC also enabled the observation of differences in deformation mechanisms resulting from the particle addition. The focus is put on the technique's potential to characterize materials and produce clear relationships between composition and mechanical strain response of any composition. The methodology proposed herein allows the observation and study of multiple deformation mechanisms from a single test, and thus can potentially minimize the number of specimens needed for a comprehensive test campaign.

Keywords: *Yield Strain Characterization, Digital image correlation, polymer toughening, epoxy toughening, particle toughening, compression testing, particle debonding, thermoset resin*

1. Introduction

Fibre reinforced composite materials are becoming increasingly established as a viable substitute for metals in high performance structural applications [1]. This change is perhaps best exemplified by the aerospace industry, whose use of composites by component weight percentage has soared in the last two decades. But, if anything else other than fabrication processes could slow down this trend, it is arguably the lack of understanding in the damage mechanics of composite systems. The high complexity resulting from the inherent heterogeneity of the microstructure causes a multiplicity of damage modes, and their interactions make the life assessment of a component very difficult. In the case of practical performance of composite structures, the matrix material is often recognized as the

limiting factor. In order to provide a laminate with serviceable properties under different loading modes, the matrix serves as a binder for the fibres, translating its properties to the entire lay-up. This is especially important for compression and low energy impact resistance as the matrix gives lateral support to the fibres under compressive loads, and absorbs energy by deforming plastically when impacted. Open hole compression (OHC) and compression after impact (CAI) tests are two of the most relevant to assess damage tolerance of a composite material. However, the requirement for high OHC (high modulus) and CAI (high toughness) strengths is incompatible for thermoset epoxy resins, which are currently the most conventional matrix material used in aerospace applications and the object of this work.

Epoxy resins display an excellent combination of mechanical properties, thermal stability and corrosion resistance; they also exhibit a relatively low degree of creep and good dimensional stability. However, the high degree of crosslinking in the polymer network after curing, precludes large conformational motion of the chains, causing the resins to be brittle. For this reason, epoxies are thermosetting materials that exhibit a glassy response at temperatures well below the glass transition temperature (T_g). Low ductility of the matrix causes laminates to have poor crack initiation and growth resistance, and consequently structures generally realize less than half of the fibre reinforcement's strength. The latter is particularly true for off-axis loading modes (hence the relevance of OHC and CAI tests). Because of this, ways of toughening the resins without compromising the modulus or T_g have been the object of assiduous research. One of the most common toughening methods is the addition of particles to the resin — with particle sizes ranging from nano to micro-scale. Toughening mechanisms in these systems can be numerous and are dependent on particle chemistry, resin chemistry and the interaction between the two [2]. According to the manufacturer, the intended toughening mechanism in the polymer systems to be used in this paper is debonding of rigid particulate fillers along with resin shear banding localized around the debonded particles. These phenomena are set to happen at stress levels below the yield stress of the neat resin, and thus act to relieve stress triaxiality by enabling dissipative plastic flow [3, 4]. Then, toughness is effectively increased at the expense of yield strength, but leaving the modulus virtually

unchanged. This improves the compromise between stiffness and ductility, and allows to continue capitalizing on the high temperature resistance of epoxy resins.

Yield behaviour characterization is central to constitutive modelling. The determination of the onset of plastic strain for polymers is not a simple task —in comparison to metals. For one thing, yielding in polymers has been shown to be highly dependent on hydrostatic pressure, strain-rate and temperature [5, 6], although the current work was limited to constant strain-rate at ambient conditions. One other innate aspect of polymers is the time dependent character of deformation; namely, viscoelastic and viscoplastic [7]. The former is active from the start of the loading and will almost completely recover in an amount of time comparable with load application; the remainder has been shown by Quinson *et al.* [8] to completely recover when heating the material to $(T_g - 20℃)$ for 1 hour. The latter becomes active once the material yields and does not recover upon load removal, that is, it develops into residual strain. It is worth noting that consensus regarding constitutive laws of finite deformation in polymers has not been reached and remains a very much active research field [7, 9-14].

The aim of this piece of research is to demonstrate the potential of digital image correlation (DIC) to study the effect that particulate filling has in the onset of residual strain and the development of the strain field; previous studies have focused on neat resin only [15]. Traditional extensometry is insufficient to capture inhomogeneous deformation, as most methods average over the gauge length. For this reason, DIC was used to track the displacement field of a random pattern applied to the surface of the specimens. The theoretical basis for image correlation can be found elsewhere [16]; put simply, DIC is the process of matching facets containing an array of grey-level values between images in a capture sequence. An interrogation area is selected for the sequence, which is in turn subdivided in what is commonly referred to as subsets. In order to aid the correlation algorithms, each unique subset should contain a monochrome pattern with a high degree of uniqueness. In order to increase the spatial resolution of the matching, subsets are overlapped (step size). When applied to mechanical testing, the matching of these facets yields a displacement vector field, and via spatial differentiation, any type of strain measure can be obtained. The ultimate goal of this operation is to produce a full-field contour map of displacement and its derivatives. The simplest form of DIC is

using one camera to calculate in-plane deformation; but as such, any out-of-plane motion will result in increased error in the measurements [17]. To help this, another camera is added to the system (3D-DIC) so that any point in the specimen's surface can be found by triangulation.

To find the onset of plastic flow, uniaxial compression loading was selected since, under tension, epoxy resins at room temperature exhibit brittle failure before yield, thus precluding the observation of yielding. The paper will describe a methodology for the measurement of strain components of epoxy resin specimens using 3D DIC; results will be presented from three unknown, but differently toughened, resin systems in order to demonstrate the potential of the method for identifying and characterising separate components of the yield response.

2. Experimental Procedure

2.1 Specimen preparation

Cylindrical specimens of epoxy resin with three compositions were provided by Cytec Engineered Materials. Namely, a neat resin (NR) and two filled resins (P1 and P2), both with 10% particle volume content but different particle types; details are not provided due to proprietary information restrictions. These restrictions are not seen as limitations since the intent is to showcase and assess the potential of DIC to study strain recovery in polymers rather than to characterize the material response. The cylinders were precision machined to a diameter of 10 mm and length of 20 mm with flat parallel ends within 0.025 mm perpendicular to the long axis. Tolerances and the length:diameter ratio are consistent with testing specification ASTM D695-10 [18]. A random pattern was applied to the curved surface using a two-stage airbrush and DecoArt Crafter's acrylic paint, thinned to a "milky" consistency with Aztek Universal Acrylic Thinner. A thin base coat of white (~30 μm) was applied to improve contrast, followed by a mist of black paint which produced speckles ranging from 3 to 25 pixels at the used magnification.

2.2 Compression testing

Tests were performed on a Tinius Olsen model H25K electromechanical frame fitted with a 25 kN load cell. The test frame was equipped with a self-aligning sub-press, model WTF-SP from Wyoming Test Fixtures[1]. Specimens were compressed at a displacement controlled rate of 1.3 mm/min as per the aforementioned specification, corresponding to a nominal strain rate of 1.083×10^{-3} s^{-1}. Compression levels of 4%, 8%, 10%, 12%, 14%, 16% and 18% as a percentage of the nominal length were applied using the analogue signal from the LVDT on the frame, starting from a preload of 10 N ± 2 N. The yield strain of the materials was known to be within this range from previous tests. Each specimen was then held at the set compression level for 10 min to obtain measures of creep. Lastly, the specimens were unloaded at the maximum crosshead speed (1000 mm/min) and left to recover for 30 minutes. Evidently, analogue data acquisition stopped after unloading. Therefore, 7 tests were

[1] Wyoming Test Fixtures Inc. 2960 E. Millcreek Canyon Rd. Salt Lake City, UT 84109, Phone: 801-484-5055, Fax: 801-484-6008, E-mail: wtf@wyomingtestfixtures.com

performed on each composition (NR, P1 and P2), providing a total of 21 datasets. Figure 1 shows an example of the longitudinal strain (in magnitude) history and the stages labelled A, B and C for the end of each load step: compression, hold and recovery, respectively.

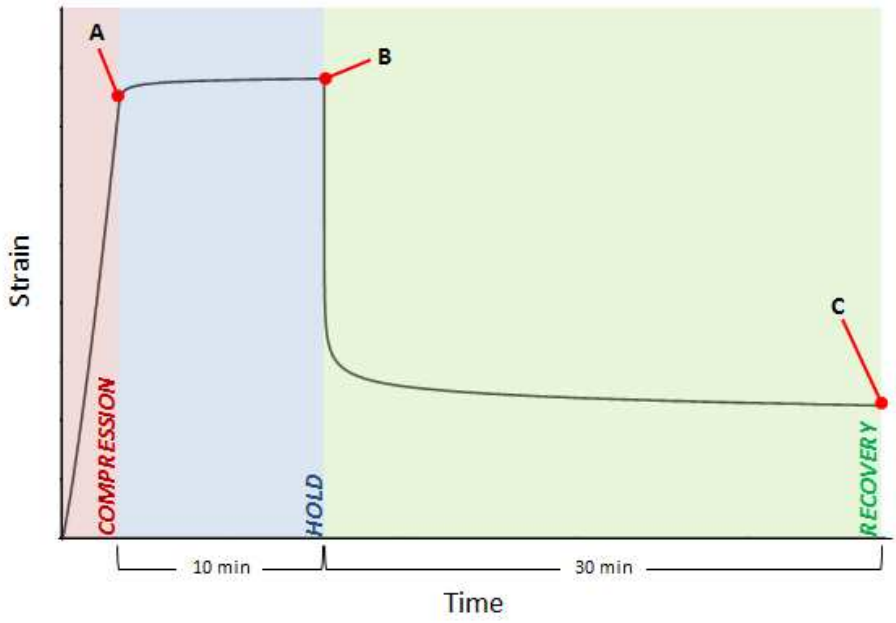

Figure 1. *Compressive strain history showing end points of each load stage: A (compression), B (hold) and C (recovery).*

2.3 DIC stereo-rig

A commercial 3D-DIC system from Limess GmbH was used with VIC-Snap software from Correlated Solutions[2] to capture the tests. High resolution (2452 x 2052 pixels) 8-bit images were captured via two 5 Megapixel CCD cameras (see Figure 2) fitted with Schneider Apo-Xenoplan 2.8/50 lenses and connected to a PC using FirewireB interface. The cameras were fixed to a t-slot aluminium profile mounted on a photographic tripod. A stereo angle of approximately 25° and magnification of 75 pixels/mm at the focal plane was used for all tests. Lens aperture was set at f/8 with exposure of 19.5 ms. Illumination was provided using two LED lamps.

In order to minimize digital data file size and processing time, the capture rate was varied depending on the load stage. That is, a low capture rate (0.5 – 1 Hz) was used for the loading stage and latter

[2] http://www.correlatedsolutions.com/

portion of the recovery segment, whereas the maximum capture rate at full resolution of the cameras (9 Hz) was used for unloading and the start of the recovery segment.

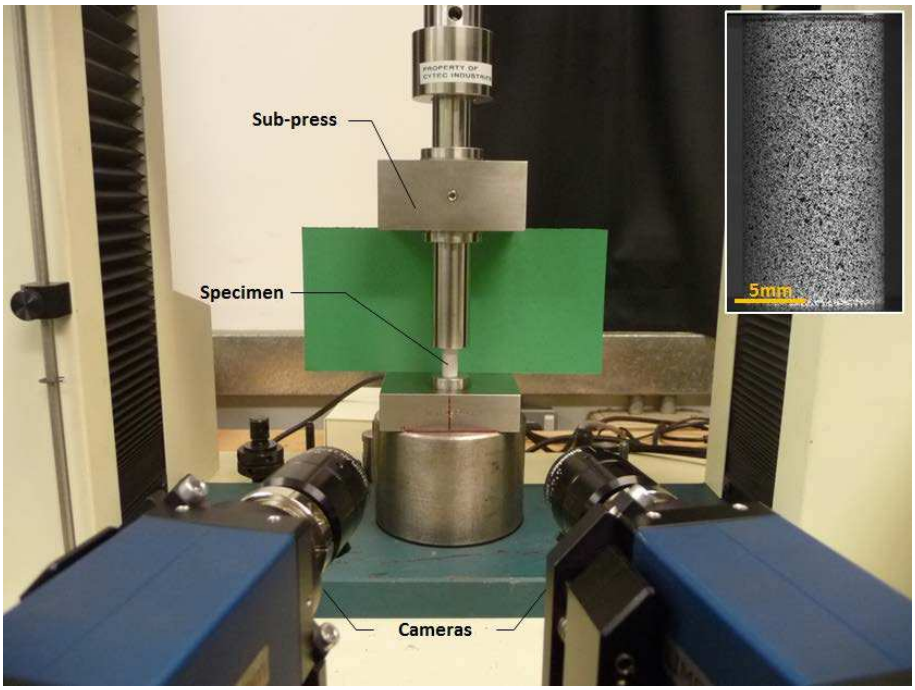

***Figure 2**. Experimental setup and painted specimen (inset).*

2.5 Uncertainty and error analysis

Image correlation was performed using the VIC-3D software from Correlated Solutions, and a 26 mm by 24 mm dot grid was used to calibrate the system. In order to get a measure of noise, two static images were captured at the beginning of each test and then digitally subtracted (per camera). Camera noise was found to be 0.94% of the dynamic range in average, *i.e.* 2.4 grey levels. The position uncertainty was calculated from triangulation of the first capture and had a mean of 0.2 μm, with range of 0.58 μm and standard deviation of 0.14 μm. The selected region of interest (ROI) for correlation covered the complete visible surface of the specimen. Matching was performed on a subset size of 29 x 29 pixels with a step size of 7 pixels. Each subset was centre-weighted using a Gaussian distribution, and matched using an affine function based on a normalized squared differences criterion [16]. Also, subsets were interpolated using an optimized 6-tap filter. The average displacement resolution from the 21 tests was 0.13 μm. Strain values were calculated using a filter size of 15 data points corresponding to a virtual strain gage of 1.32 mm (99 pixels). Strain measurements used for the analysis were taken from the central portion of the ROI since data from the edges of the specimen

have increased noise due to low light artefacts and poor focus. The average strain resolution was then equal to 95 μm/m. A final verification of the spatial matching was done by applying a coordinate transformation to a best fit cylinder for which the average diameter was 10.07 mm. This was consistent with measurements made with a micrometre on the painted specimen within 0.05%.

3. Results

3.1 Strain Measurements

The Cauchy definition was used to compute deformation, *i.e.* the normal compressive strain and the normal transverse strain are given by $\varepsilon_c = \left|\frac{l-l_0}{l_0}\right|$ and $\varepsilon_t = \frac{d-d_0}{d_0}$, respectively. Note that the compressive strain is given as magnitude; l and d are the actual length and width, whereas subscript "0" indicates initial dimensions. It is acknowledged that engineering strain will deviate from true strain at large deformation levels, however, this decision was justified on the grounds of the objective for this research: the intent is to showcase and assess the potential of DIC to study strain recovery in polymers rather than to characterize the material response. Additionally, the choice of a nominal strain definition saved processing time and can be compared readily with traditional extensometry.

A number of avenues are available for the determination of the yield strain, the simplest of which is the extraction of longitudinal strain, ε_c, by means of a virtual extensometer laid over the specimen's length, thereby neglecting the full field capacity of DIC; this data can, nonetheless, be readily compared with more conventional instruments like strain gauges or a machine's LVDT. Similarly, a second approach is to average strain over an interrogation area. This yields a more inclusive measure of strain, but by averaging the strain gradient within the interrogation area neglects variation from non-homogeneous deformation. In order to include such variation, data can be extracted locally from a set of points across the correlated data (third approach). Strain values were then extracted as per the second and third methods, to get global and local measurements, respectively. Data from each method was used to construct a double ordinate plot of nominal axial stress or residual strain vs. normal compressive strain (see Figures 3 and 4). The onset of plastic deformation was then determined by linear back-extrapolation of the non-zero residual strain points. The goodness of fit was quantified in terms of the coefficient of determination R^2. In turn, the nominal yield stress is determined from the stress value at the intersection with the abscissa. Then, nominal compressive stress is defined as $\sigma_c = \frac{F}{A_0}$, where F is the analogue force signal and A_0 is the nominal cross-sectional area of the specimen.

During the tests, some problems arose from the load deviating from axiality, particularly at compression levels > 10%. Even with the use of the self-aligning sub-press, specimen developed a significant amount of shear strain which is indicative of uneven loading, which was confirmed by non-axisymmetric normal strain fields. Whereas a small amount of looseness in the sub-press assembly could have contributed to this, frictional forces at the loading surfaces is the most probable cause. It is well known from forming of metals that deformation under compression is highly dependent on the tribology of the loading interface, with the amount of bulging or "barrelling" being proportional to the friction coefficient [19]. It has also been shown in other studies that frictional forces oppose the development of hoop strain near the ends of cylindrical specimens while reaching a maximum at half the height [20, 21]. It follows then, that the stress state near the ends of the cylinder approximate one resulting from pure hydrostatic pressure. Another consequence of this "arrest" is the formation of acute strain gradients at the ends, larger in magnitude for longitudinal strain, and that transverse deformation is nonhomogeneous over the length of the specimen. For these reasons we did not deem it sensible to report Poisson's ratio, since stress states are effectively different at the ends and half the height. This lack of true load alignment then further supported the case for comparison of local vs. global results. The non-homogeneous transverse deformation can be greatly alleviated with the use of lubricant or PTFE tape [22], but we performed the tests without lubrication. The sub-press we used displayed a slight deviation from axiality which could have resulted in the specimen slipping. The main reason for not using lubrication at the load interfaces was to prevent rigid body motion at high strain levels. Also, it was decided to use the normal compressive strain only for the determination of the yield point, although the use of additional metrics (transverse or equivalent strain) remains as a possibility for future communications.

Creep and stress relaxation were also investigated for each compression level and plots of strain and stress development after 10 minutes (from stage A to B) were produced for each resin system (Figures 5 and 6).

3.2 Yield behaviour

The stress-strain curves for the 3 resin systems are shown in Figure 3, along with residual strain values, at the right ordinate axis. It is apparent that particulate filling (P1 and P2) affects the yield behaviour of the neat resin (NR), namely a decrease was observed in both the yield stress and the onset of plastic strain. However, the modulus of the P1 system was almost equal to the neat resin, whereas it was lower for the P2 system. Only the P1 composition displayed a very shallow load drop after yield before continuing to strain harden. Also, from the nominal stress – strain curves it can be observed that P1 exhibited the most repeatable load response over the 7 compression levels, followed by NR and P2, respectively. The residual strain value sets after the 30 minute recovery approximated nicely the expected bilinear shape. Still, the relatively short duration of the recovery phase capture left a significant amount of anelastic strain yet to recover, seen as non-zero points at lower than yield strains. Findings by Quinson *et al.* [8] show that the onset of plastic strain in amorphous glassy polymers is independent of recovery time beyond a timescale comparable with loading, only the 3 data points corresponding to the highest compression levels for each system were used to fit a line to intersect the abscissa. From that, the macroscopic yield stress was found by averaging the stress values at the intersection.

The specimens could have been heated to $T_g - 20℃$ so as to remove all anelastic strain in order to corroborate the onset of plasticity, but the need for manipulation of the specimen would have resulted in added error from the correlation after. Instead, we verified the yield point by constructing another double ordinate plot using point measurements of a grid of 3 by 12 points laid across the hoop and axial directions, respectively, covering the breadth of the ROI. The sets of 26 residual strain points per compression level are plotted in Figure 4. Again, the datasets displayed a nearly bilinear shape and the same hierarchy of unrecovered anelastic strain. The linear fit was performed by maximizing the goodness of fit of the non-zero residual strain values, in the same fashion as the macroscopic values. That is, points closely below yield were deemed to be unrecovered anelastic deformation, and were excluded from the fit. Values for yield strain and stress, R^2 and the percentage difference between both measurements are shown in Table 1. Understandably, noise affected more the local measurements, which was translated into scatter; hence, the lower coefficients of determination. However, note that the marker size for the data sets in Figures 3 to 6 is significantly larger than the

standard deviation of the uncertainty (strain resolution = 95 micro strain), thus showing the error bars would be impractical. Nonetheless, there is relatively low difference in the yield points found by the two methods, for all values but the yield strain of the neat resin. The neat resin displayed the highest stiffness so that the number of compression levels tested may have been insufficient to resolve more clearly the plastic segment of the macroscopic dataset. As such, the lowest strain value from the 3 used to find the onset of plasticity in the neat resin is very likely anelastic deformation only, resulting in a lower onset value. Regardless of this, the veracity of the values found with the local method is substantiated by the close agreement in the filled resins results.

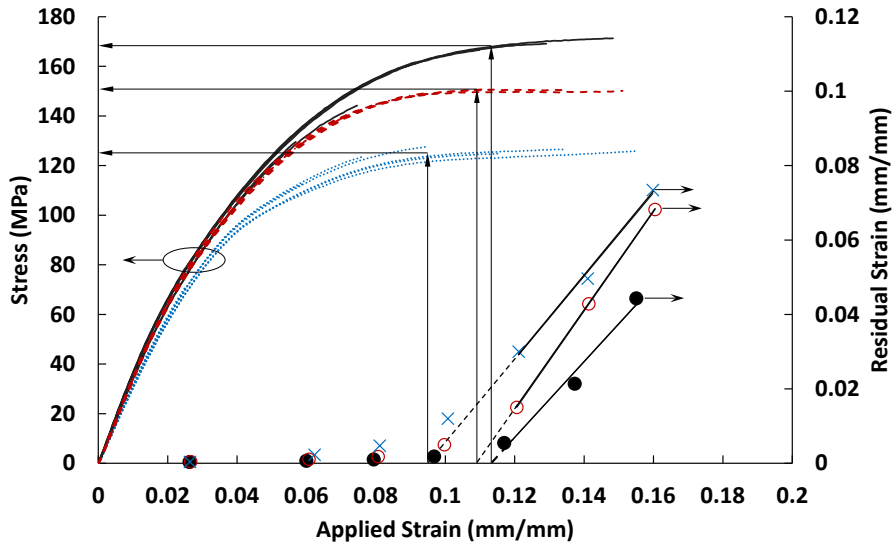

Figure 3. *Yield point location for NR (— , ●), P1 (--- , ○) and P2 (⋯ ,×) based on nominal axial strain and nominal compressive stress.*

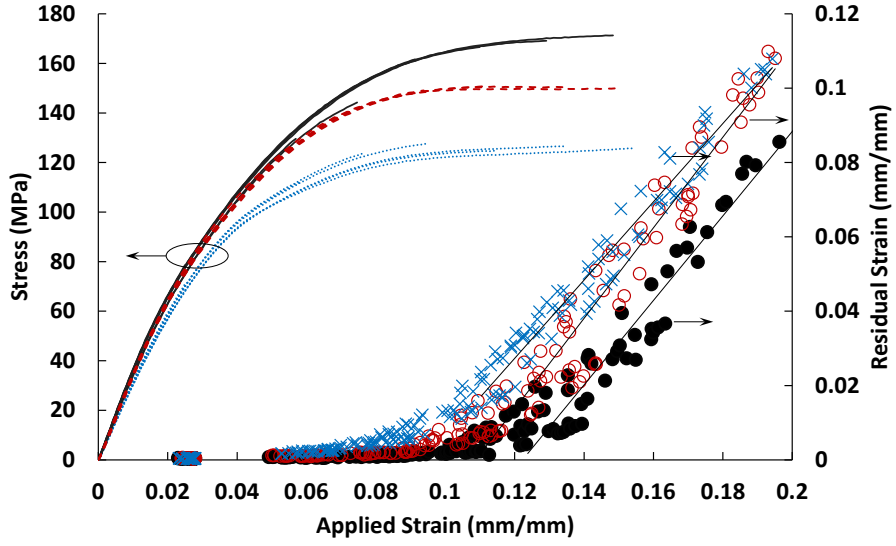

***Figure 4**. Yield point location for NR (— , ●), P1 (--- , ○) and P2 (··· , ×) based on local axial strain values and nominal compressive stress.*

***Table 1**. Yield point of each resin system based on macroscopic and local measurements.*

	MACROSCOPIC		LOCAL		% DIFFERENCE	
	ε_{yield}	σ_{yield} (MPa)	ε_{yield} (R^2)	σ_{yield}	ε_{yield}	σ_{yield}
NR	11.31% (R^2 = 0.98)	167.7	12.23% (R^2 = 0.95)	168.6	7.4%	0.5%
P1	10.94% (R^2 = 0.99)	150.2	10.85% (R^2 = 0.94)	149.9	0.8%	0.2%
P2	9.52% (R^2 = 0.99)	124.9	9.41% (R^2 = 0.96)	126.2	1.3%	1.0%

3.3 Creep and stress relaxation

Macroscopic values for creep and stress relaxation during the segment AB (compression hold) of the tests are shown in Figure 5. Both responses appear to be enhanced by the addition of particles, albeit only beyond a certain deformation level. There is virtually no difference in the relaxation response for applied strains below ~8%, whereas at higher strain levels the P2 system exhibited the least amount of relaxation, followed by P1 and the neat resin, respectively. Due to the small magnitude of the levels measured, noise had a much greater effect on creep data. Still, a similar trend to relaxation was observed, with the neat resin creeping the most and P2 the least. Again, composition seems to have no effect on the creep response for strain levels below ~10%. Note that for each system, both time dependent responses seem to approach a constant value at higher strains, but these trends can only be further elucidated by performing test repeats.

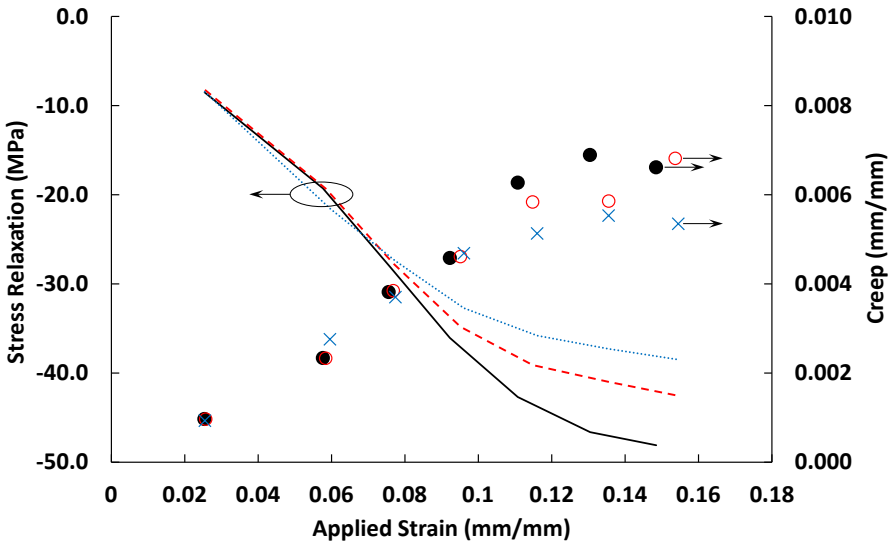

***Figure 5**. Compressive stress relaxation and nominal axial creep during stage A-B (compression hold) for NR (— , ●), P1 (--- , ○) and P2 (··· , ×).*

Local creep values were also obtained using point measurements as shown in Figure 6. As stated before, material near the load interfaces approximates a hydrostatic stress state so that Poisson's ratio does not remain constant over the length of the specimen. Then, the high degree of scatter in the local creep data is likely a consequence of this; but despite this dispersion, the same hierarchy between compositions can be recognized. It also was observed that at certain strain levels some points in the specimen recovered, thus the negative creep values. Upon inspection it was found that for the neat resin these points corresponded to the top portion of the specimen at 18% compression. As it will be seen in Section 3.4, during this test, the middle portion of the specimen underwent the highest deformation. The tractive forces at the load interfaces caused the specimen to deform in-homogeneously and to start yielding away from the ends first. The accretion of this plastic zone thus caused a significant portion of the specimen to have a lower modulus than the material at the ends. A consequence of this is that the material at the ends recovered during the load hold instead of developing more strain, while the middle continued to deform plastically. The same phenomenon was observed in the filled resins, where P1 exhibited local recovery at strains as low as 5% and P2 as low as 8.2%. But then again, these clusters of negative creep points seem to be centred at the yield point, which is consistent with their location in the specimens, namely away from the zone were the majority of the plastic flow is taking place, hence resulting from load transfer within the specimen. It can be

also be noted that this local recovery at constant compression maintains the same ranking, with the P2 composition displaying the least amount of recovery by magnitude, and the neat resin the most.

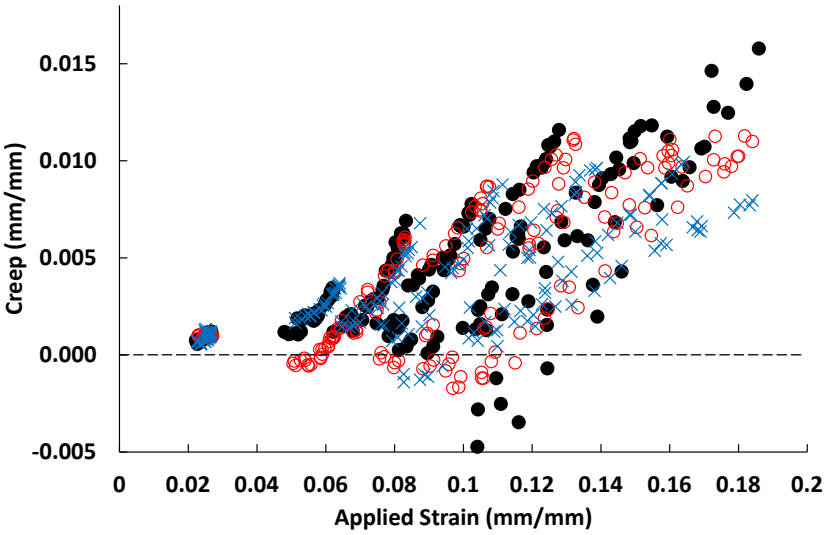

***Figure 6**. Local axial creep values during stage A-B (compression hold) for NR (●), P1 (○) and P2 (×).*

3.4 Strain components

Using data from the recovery segment of each test, the total strain was resolved into its strain components based on the nature of their recovery, namely elastic, plastic and anelastic. It has already been shown what was taken as the plastic strain. Then, the second time derivative of the first 10 seconds of the recovery stage was used to find the elastic component of the deformation, which was defined as the total strain minus the strain at the time where the second derivative is maximum, *i.e.* at the largest change in slope. It is acknowledged that the results are not purely elastic, as deformation in polymers has been extensively shown to be time-dependent, and therefore viscous flow is prevalent in the mechanical response of the material. To clarify this figures 7 to 9 show the recovered strain during the first 10 seconds after the load was released (see Figure 1 stage B) for the 3 systems. Note that all datasets were offset to zero at the start of the recovery and labelled according measured applied strain for identification. It can be seen that the time dependency of the strain recovery increases markedly after yielding and that, in turn, the amount of deformation that is recovered immediately decreases in proportion to the yield point.

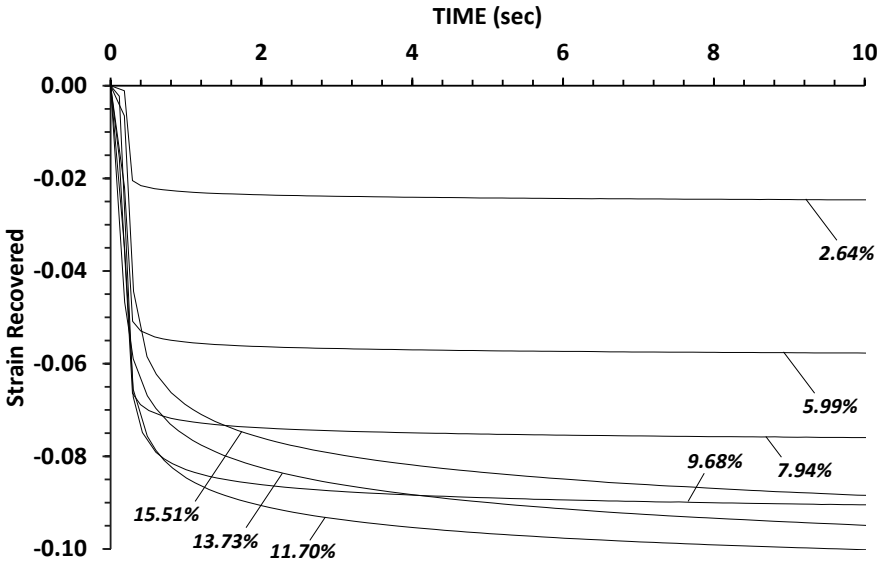

***Figure 7**. Axial strain recovery after 10 seconds of the load release for NR. Labels indicate the average applied strain at the end of the load hold (Stage B) as measured by an interrogation window.*

The dataset corresponding to the P1 coupon tested at 16% LVDT compression which corresponded to an applied axial strain of 14.14% (see Figure 8) was sampled at a lower rate (1 Hz) than the rest of the tests due to problems with the electronic shutter in the system.

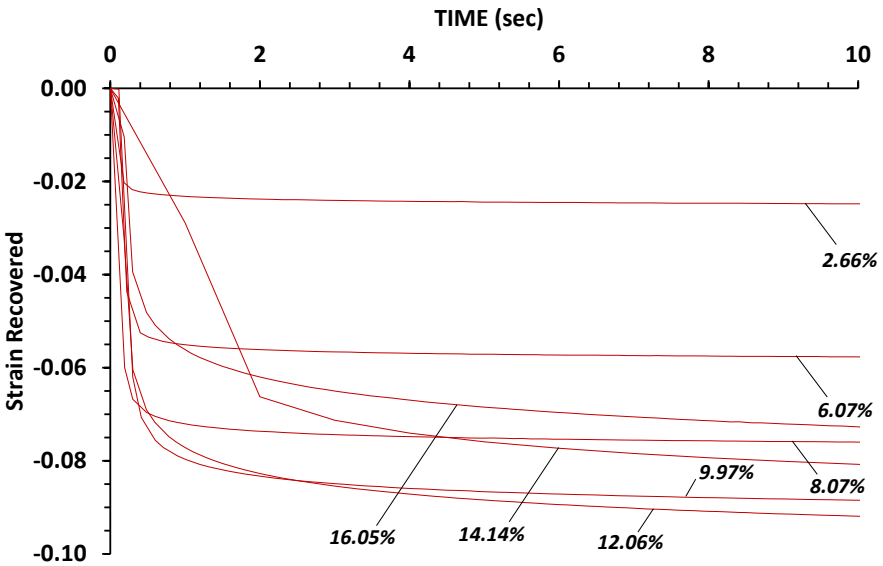

***Figure 8**. Axial strain recovery after 10 seconds of the load release for P1. Labels indicate the average applied strain at the end of the load hold (Stage B) as measured by an interrogation window.*

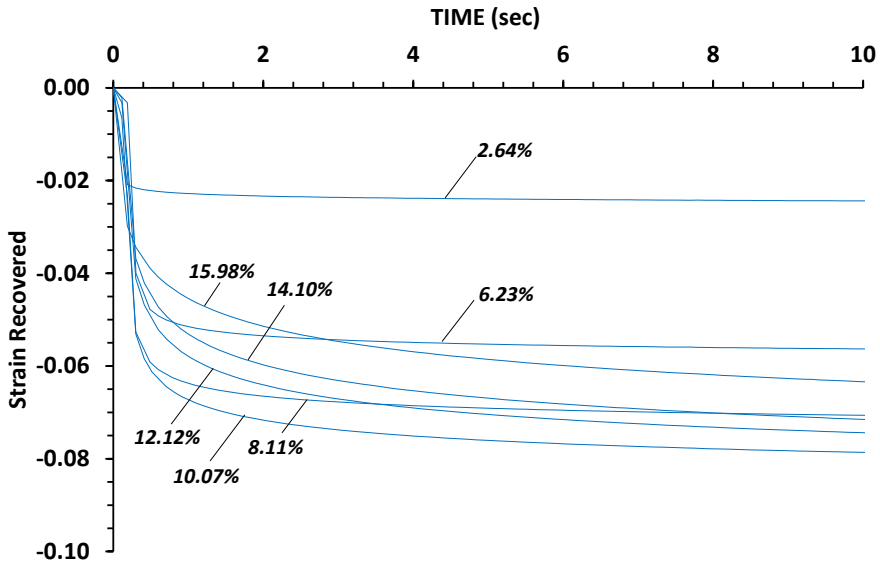

***Figure 9**. Axial strain recovery after 10 seconds of the load release for P2. Labels indicate the average applied strain at the end of the load hold (Stage B) as measured by an interrogation window.*

Although other authors have used the unrelaxed modulus to calculate elastic strain [8], we did not possess this information and believe that our method provides a valid estimation of the elastic recovery trend.

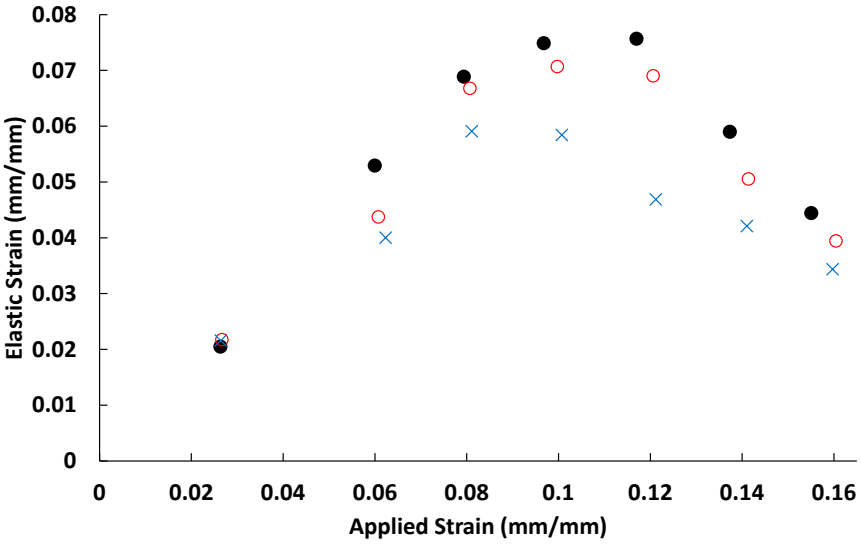

***Figure 10**. Elastic component of nominal axial strain for NR (●), P1 (○) and P2 (×).*

As shown in Figure 10, findings are consistent with observations from the stress-strain curves and the recovery histories shown in Figures 7 to 9, where the neat resin and the P1 system display the highest

similarity in modulus. As expected, the ranking in elastic response over the tested deformation range is consistent with other measurements. However, the elastic component seems to be independent of composition at strains < 3%, and also appears to converge at the higher strain levels. The curves for the 3 systems display a concave shape, with the maximum corresponding approximately to the onset of plastic strain.

Anelastic strain was then calculated as $\varepsilon_{an} = \varepsilon_t - \varepsilon_{pl} - \varepsilon_{el}$, where the right side terms correspond to total, plastic and elastic strains, respectively; results are shown in Figure 11. It can be seen that the anelastic component of deformation is active from the start of the loading for the 3 systems. Again, particulate filling appears to have a negligible effect in the mechanical response at strains below 3%. Only the neat resin displays a monotonic increase over the compression range, while the filled resins exhibit a small local departure at ~6% strain. Although it is expected that the anelastic strain will reach a maximum, it is difficult to anticipate the component curve trend, unless higher compression tests are performed. Nonetheless, both filled resins ostensibly reach this anelastic plateau at lower strains than the neat resin, which is likely a consequence of the increased plastic flow dissipation enabled by the particles debonding.

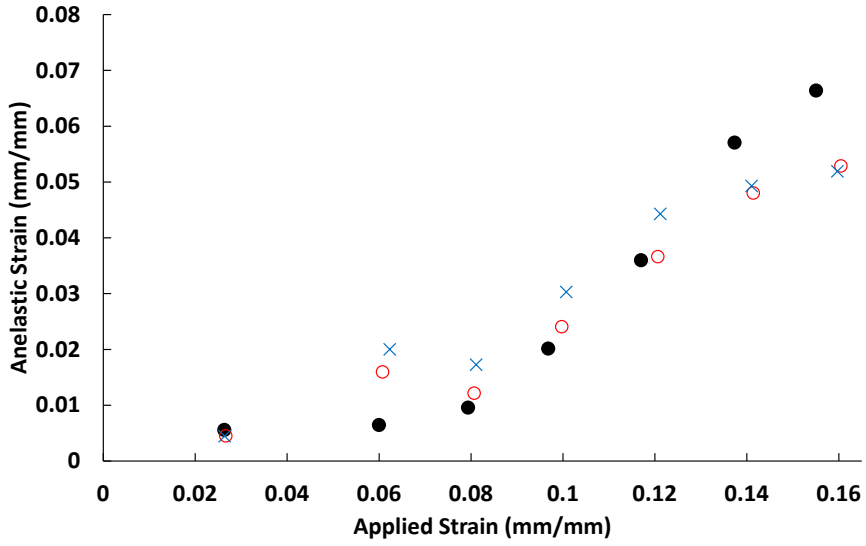

Figure 11. *Anelastic component of nominal axial strain for NR (●), P1 (○) and P2 (×).*

3.5 Strain maps

The full field strain maps at the stages defined earlier are shown from Figures 12 to 14, for the 3 resin systems, respectively. Although specimens are different for each compression level, a definite trend in the deformation levels of the different compositions can be observed. Namely, that strain gradients are markedly more pronounced in the neat resin specimens, causing a more localized plastic zone (see stage C at 18% in Figure 12). The filled resins exhibited more homogeneous strain fields, resulting in larger plastic zones in comparison to the neat resin. Although this is done at the expense of yield strength, it can be seen that the viscoelastic regime remains nearly unchanged. Another important observation enabled by the use of DIC was the difference in the toughening mechanism of the two filled resins. Localized strain gradients were found distributed randomly over the P2 specimens (see Figure 14), more distinguishable at compression levels > 10%.

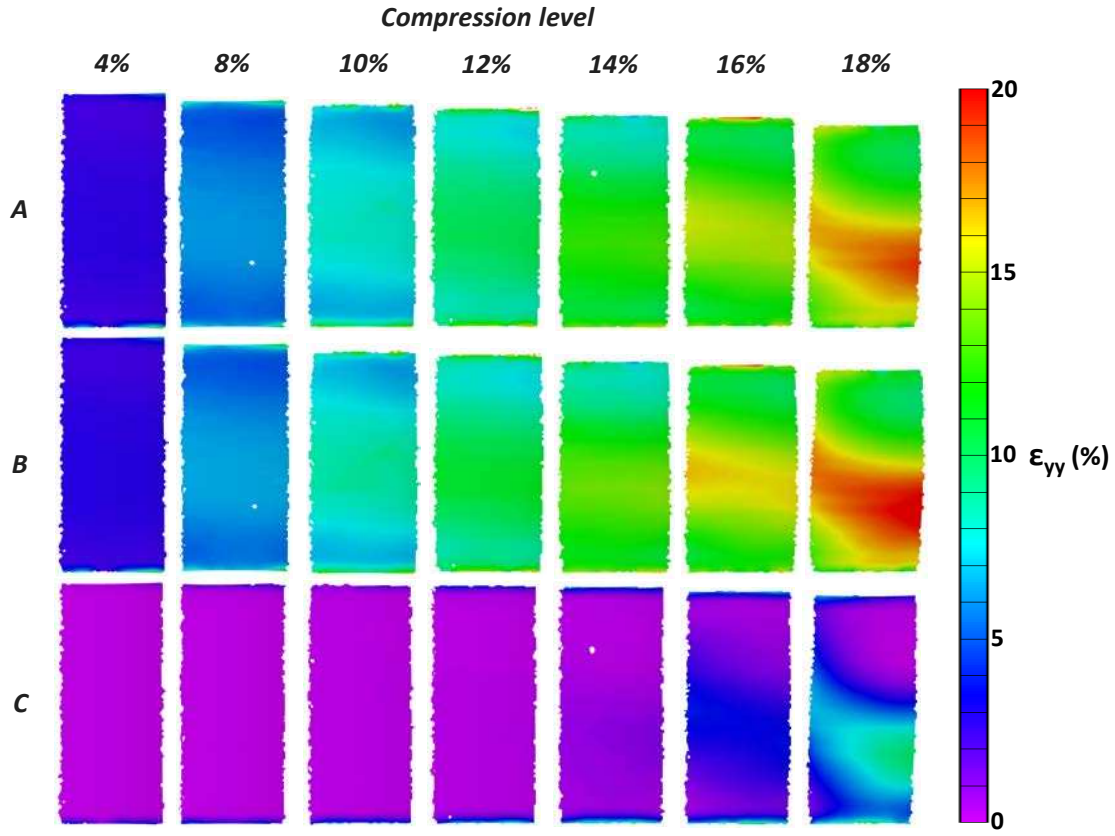

Figure 12. *Neat resin strain maps at different LVDT compression levels.*

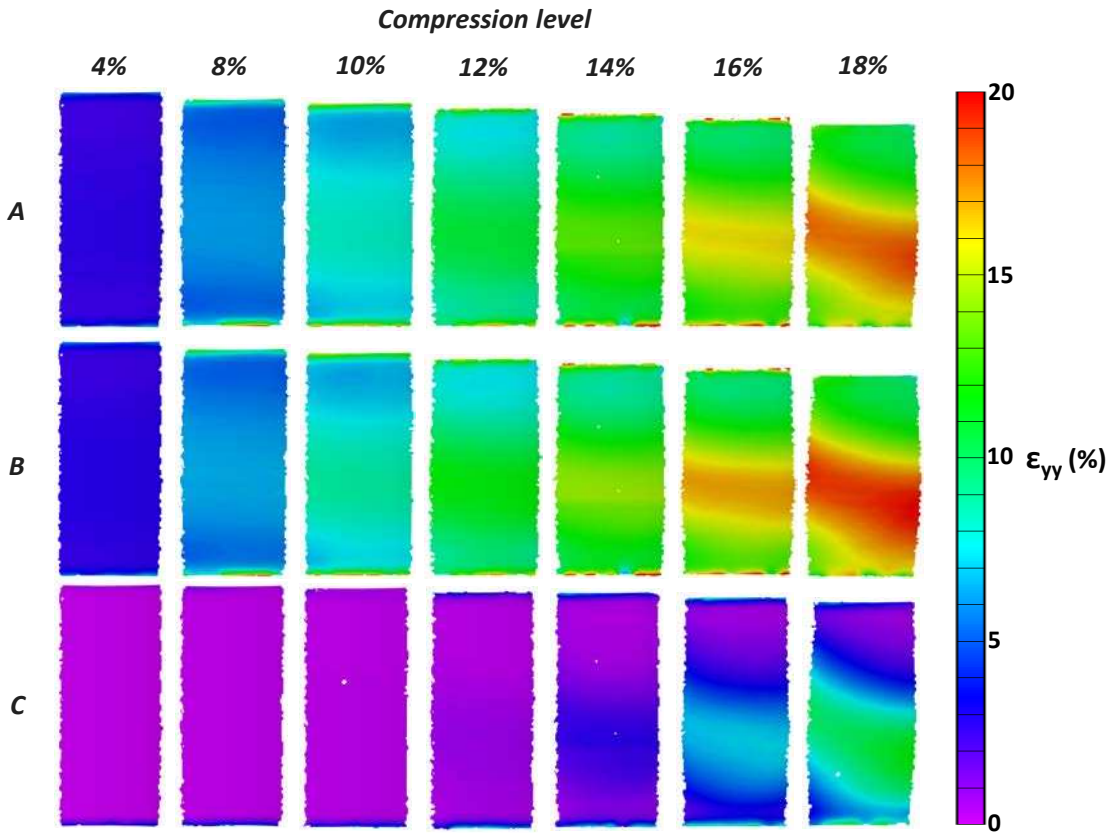

***Figure 13**. P1 resin strain maps at different LVDT compression levels.*

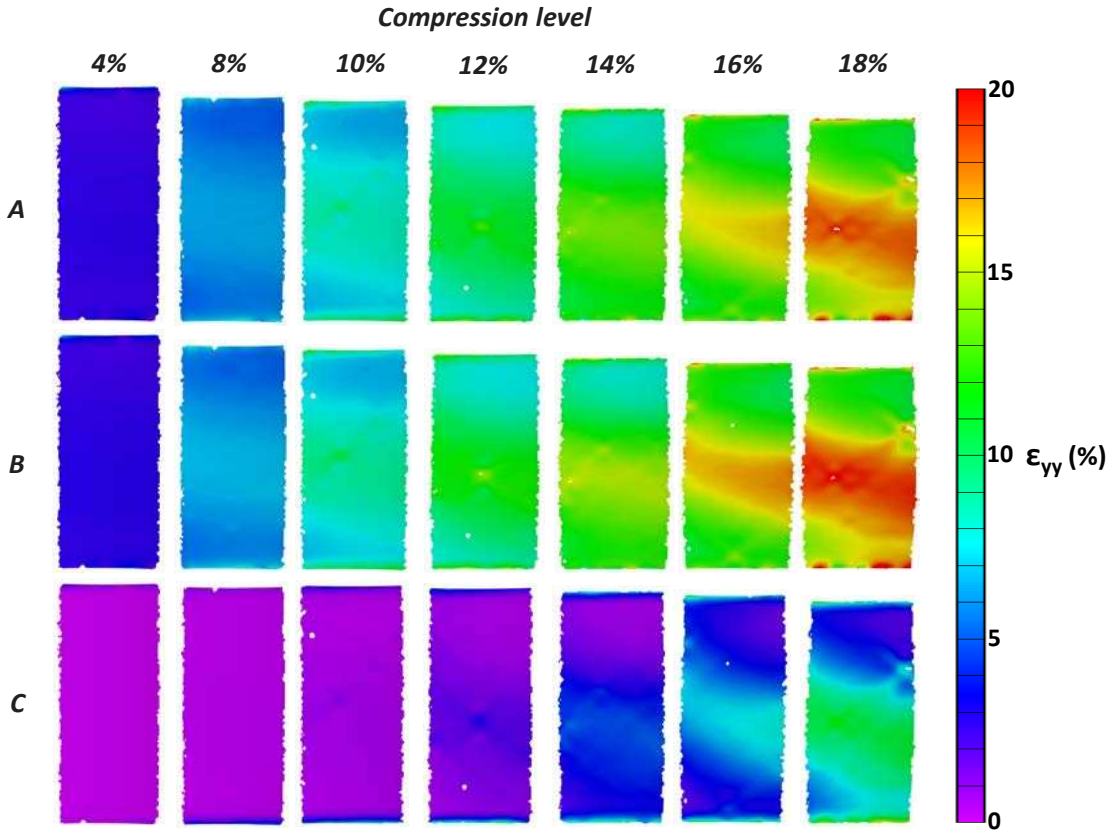

***Figure 14**. P2 resin strain maps at different LVDT compression levels.*

These gradients may be seen in closer detail in Figure 15 which shows maps of shear strain, ε_{xy}, of material P2 tested at 18% LVDT compression. The "x-shaped" gradients are in fact acute shear bands likely caused by plastic void growth resulting from particle debonding. This hypothesis was further supported by uncorrelated zones at the centre of these gradients, which is often an indication of cracks. No such localized gradients were found in P1 maps. However, since details of the particles, *i.e.* size and composition, are not provided, it is difficult to draw conclusions related to the actual mechanism of plastic flow dissipation. Also, as the distribution of particles within the specimen is random, it cannot be known the radial location of a particle solely from the local strain state. Hence, a sufficiently large number of specimens would need to be tested and compared, if a clear trend is to emerge. Nevertheless, these results demonstrate the potential of 3D DIC to provide more detailed full-field strain information which materials developers may use in the future to enhance the understanding of how particles dissipate energy.

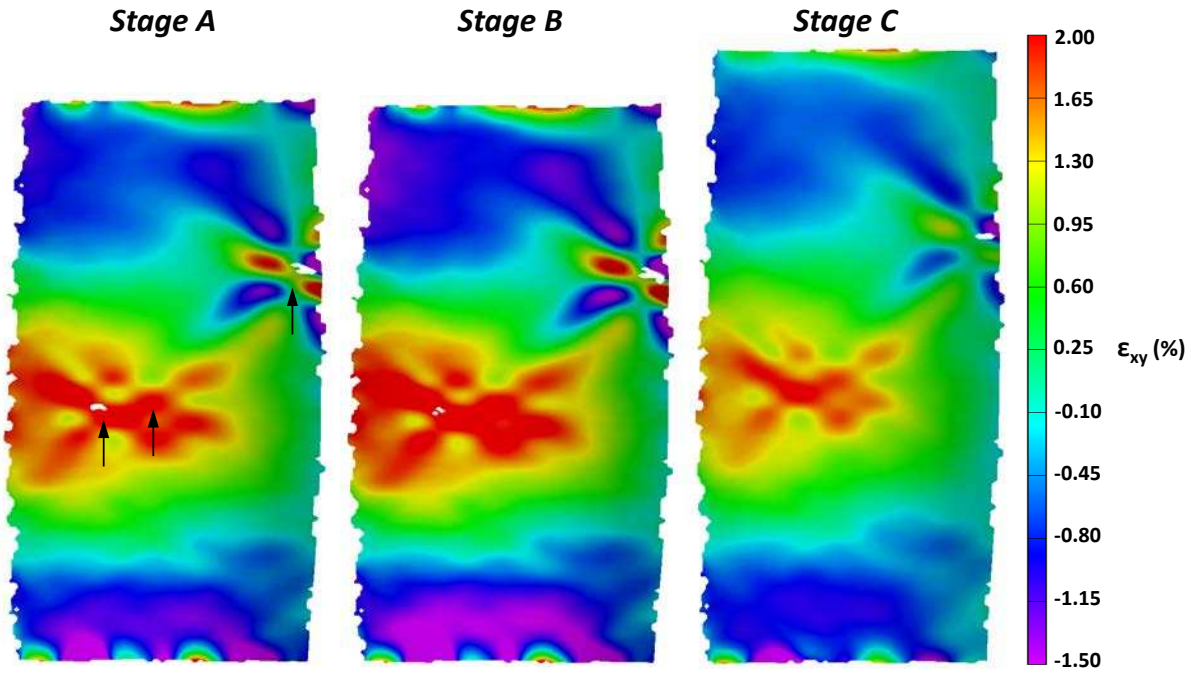

***Figure 15**. Maps of shear strain showing much localized shear bands around what appears to be plastic void growth resulting from debonded particles (arrows). This specimen is P2 tested at 18% LVDT compression.*

4. Discussion and Conclusion

A method to measure strain recovery and time dependent response using a uniaxial compression test was introduced. In conjunction with 3D-DIC, the method proved to be effective in studying the yield behaviour, creep and stress relaxation of these materials. The full field strain maps also provided valuable information regarding the deformation mechanisms.

The yield points of two filled resins and the neat resin were successfully obtained by finding the onset of plastic strain from local and global measurements; both scales yielded similar results, supporting the case for their validity. It would not have been possible to find the yield point otherwise as the stress-strain curves did not display the traditional “knee”, and also because of the large amount of anelastic deformation active during loading. Due to proprietary restrictions, details of the polymer network and blends were not provided. However, even without details for the particles, their effect on modulus and macroscopic nominal stress is clearly apparent. Particulate filling reduced the yield strength of the neat polymer, but only the modulus of the P2 blend was lower. It was also shown that, whatever the difference in composition, the filled resins displayed a reduced degree of localization in the deformation field. This is seen more clearly in the strain maps in Section 3.4 (Figures 12-15), but it can also be inferred from the lower amount of scatter in the creep response of the blends as shown in Figure 6. By becoming active at lower strains, the particulate fillers were also seen to help the macroscopic creep and stress relaxation response, thus improving the dimensional stability of the resin. It was also possible to study the development of the strain components, albeit qualitatively as the unrelaxed modulus of the resins was not known and the specimens were only allowed to recover for 30 minutes. Nonetheless, it was possible to observe that the viscoelastic component of deformation is always present and approaches a steady value after the material has undergone macroscopic yielding. By contrast, elastic deformation will decrease steadily in magnitude after macroscopic yield has taken place.

The study of heterogeneous deformation fields is much more arduous with other experimental techniques such as traditional extensometry, photoelasticity or moiré interferometry, whereas comparison of strain gradients and concentrations are readily made with DIC. Even with relatively

low bit-depth images, it was possible to make observations of what appears to be microscopic plastic void growth. In order to fully capitalize from this capacity, the coordinates of the particles would need to be either known or controlled *a priori*.

Another major benefit of using a full field technique is the capacity to corroborate relationships by extracting local measurements. For instance, the onset of plastic deformation and creep response was verified using local values. It is apparent that the technique may be used to approximate volumetric strain measurements from calculations of Poisson's ratio, and thus can be useful to observe the degree of compaction caused by different particle composition. Due to large frictional forces at the loading interfaces, it was not possible to achieve homogeneous transverse deformation, and therefore, realistic volumetric measurements would only be possible by obtaining data from the whole circumference of the specimens, *i.e.* setting 4 pairs of cameras around the specimen.

Sensitivity to strain-rate, temperature and hydrostatic pressure, in addition to the time-dependency of the mechanical response, greatly complicates the characterization of polymeric materials and prompts for efficient testing methodologies that can provide a comprehensive description of the material response whilst remaining practical. It has been demonstrated that the technique presented here can characterize efficiently the different components of yield behaviour and can provide full-field strain information which may be used in understanding the toughening mechanisms resulting from particle addition. By undertaking "blind" tests here, enabled an unbiased presentation of the different materials tested. We were not able to connect the properties observed with the structure of the unknown materials, but that was not the aim of the work. Materials developers, with knowledge of the structure of their materials, may use this methodology as a tool to discern structure-property relationships. The methodology can be tailored to reduce the testing time or improve the trend capture, namely by varying the number of compression levels and duration of the load hold and recovery. We believe that the method used to resolve strain components can produce realistic trends, provided that the camera capture rate is sufficient and test repeats are performed to validate such results.

The development of this work inevitably raised caveats for future work. The increased amount of shear stress caused by load deviating from axiality was a major nuisance as it precluded the obtainment of an axisymmetric load distribution. This along with the arrest of material near the ends caused by large frictional forces, caused the specimens to develop a highly heterogeneous deformation field. It has been shown in other studies [22] that by minimizing these two problems, the specimen will deform symmetrically and thus yield better relationships between load and strain. Also, provided that the specimen can be heated to remove all anelastic strain without increasing error in the measurements, the need for an unpractically long recovery time is eliminated. Perhaps the potential for the study of deformation fields around particles used in toughening is the most enticing aspect of this work, as it not only reduces the cost involved in doing this with tomographic techniques but also the post processing time and complexity. Overall data on yield strain, using the method described here can be readily used to anticipate unrecoverable deformation based on nominal dimensions, i.e., without the need to know beforehand or measure the instantaneous dimensions of the structure to be designed.

5. ACKNOWLEDGEMENTS

This research was supported in kind by Cytec Aerospace Materials. Funding for this research was kindly provided by the National Council of Science and Technology of Mexico (CONACyT).

6. References

[1] C. Soutis, "Carbon fiber reinforced plastics in aircraft construction," *Materials Science and Engineering: A,* vol. 412, pp. 171-176, 2005.

[2] G. Borstnar, M. Mavrogordato, L. Helfen, I. Sinclair, and S. Spearing, "Interlaminar fracture micro-mechanisms in toughened carbon fibre reinforced plastics investigated via synchrotron radiation computed tomography and laminography," *Composites Part A: Applied Science and Manufacturing,* vol. 71, pp. 176-183, 2015.

[3] A. Kinloch, R. Mohammed, A. Taylor, C. Eger, S. Sprenger, and D. Egan, "The effect of silica nano particles and rubber particles on the toughness of multiphase thermosetting epoxy polymers," *Journal of Materials Science,* vol. 40, pp. 5083-5086, 2005.

[4] R. A. Pearson and A. F. Yee, "Influence of particle size and particle size distribution on toughening mechanisms in rubber-modified epoxies," *Journal of Materials Science,* vol. 26, pp. 3828-3844, 1991.

[5] M. C. Boyce, D. M. Parks, and A. S. Argon, "Large inelastic deformation of glassy polymers. Part I: rate dependent constitutive model," *Mechanics of Materials,* vol. 7, pp. 15-33, 1988.

[6] E. M. Arruda, M. C. Boyce, and R. Jayachandran, "Effects of strain rate, temperature and thermomechanical coupling on the finite strain deformation of glassy polymers," *Mechanics of Materials,* vol. 19, pp. 193-212, 1995.

[7] O. Hasan and M. Boyce, "A constitutive model for the nonlinear viscoelastic viscoplastic behavior of glassy polymers," *Polymer Engineering & Science,* vol. 35, pp. 331-344, 1995.

[8] R. Quinson, J. Perez, M. Rink, and A. Pavan, "Components of non-elastic deformation in amorphous glassy polymers," *Journal of materials science,* vol. 31, pp. 4387-4394, 1996.

[9] A. Argon, "A theory for the low-temperature plastic deformation of glassy polymers," *Philosophical Magazine,* vol. 28, pp. 839-865, 1973.

[10] C. Buckley and D. Jones, "Glass-rubber constitutive model for amorphous polymers near the glass transition," *Polymer,* vol. 36, pp. 3301-3312, 1995.

[11] S. G. Bardenhagen, M. G. Stout, and G. T. Gray, "Three-dimensional, finite deformation, viscoplastic constitutive models for polymeric materials," *Mechanics of Materials,* vol. 25, pp. 235-253, 1997.

[12] A. Khan and H. Zhang, "Finite deformation of a polymer: experiments and modeling," *International Journal of Plasticity,* vol. 17, pp. 1167-1188, 2001.

[13] O. U. Colak, "Modeling deformation behavior of polymers with viscoplasticity theory based on overstress," *International Journal of Plasticity,* vol. 21, pp. 145-160, 2005.

[14] E. Ghorbel, "A viscoplastic constitutive model for polymeric materials," *International Journal of Plasticity,* vol. 24, pp. 2032-2058, 2008.

[15] S. Heinz, J. Tu, M. Jackson, and J. Wiggins, "Digital image correlation analysis of strain recovery in glassy polymer network isomers," *Polymer,* vol. 82, pp. 87-92, 2016.

[16] M. A. Sutton, J. J. Orteu, and H. Schreier, *Image correlation for shape, motion and deformation measurements: basic concepts, theory and applications*: Springer Science & Business Media, 2009.

[17] M. Sutton, J. Yan, V. Tiwari, H. Schreier, and J. Orteu, "The effect of out-of-plane motion on 2D and 3D digital image correlation measurements," *Optics and Lasers in Engineering*, vol. 46, pp. 746-757, 2008.

[18] ASTM, "Standard test method for compressive properties of rigid plastics," in *Annual Book of ASTM Standards, Designation D695-10*, ed, 2010.

[19] C. Lee and S. Kobayashi, "New solutions to rigid-plastic deformation problems using a matrix method," *Journal of Manufacturing Science and Engineering*, vol. 95, pp. 865-873, 1973.

[20] J. Banerjee, "Barreling of solid cylinders under axial compression," *Journal of Engineering Materials and Technology*, vol. 107, pp. 138-144, 1985.

[21] F.-K. Chen and C.-J. Chen, "On the nonuniform deformation of the cylinder compression test," *Journal of engineering materials and technology*, vol. 122, pp. 192-197, 2000.

[22] M. Jerabek, Z. Major, and R. Lang, "Uniaxial compression testing of polymeric materials," *Polymer testing*, vol. 29, pp. 302-309, 2010.